

Subgap biasing of superconducting tunnel junctions without a magnetic field

K. Segall,^{1,b)} J. Moyer,^{1,a)} and Juan J. Mazo²

¹Department of Physics and Astronomy, Colgate University, Hamilton, New York 13346, USA

²Departamento de Física de la Materia Condensada and ICMA, CSIC-Universidad de Zaragoza, Zaragoza 50009, Spain

(Received 8 January 2008; accepted 21 June 2008; published online 29 August 2008)

Superconducting tunnel junctions (STJs) have been successfully used as single-photon detectors but require the use of a magnetic field to operate. A recent paper has proposed the idea to use a circuit of three junctions in place of a single junction in order to achieve the necessary biasing without applying a magnetic field. The nonlinear interaction between the different junctions in the circuit causes the existence of a stable subgap state for one of the junctions, which acts as the detector junction. In this paper, we present the first measurements demonstrating the existence of such a biasing state feasible for STJ detectors. Single junction measurements with an applied magnetic field help determine the functional form of the subgap current versus voltage; then the operating point of a three-junction circuit is measured and fit to theory. The excellent match between theory and experiment demonstrates the existence of the subgap biasing state. The outlook for possible use in detector applications is discussed. © 2008 American Institute of Physics.

[DOI: 10.1063/1.2970159]

I. INTRODUCTION

The use of superconducting tunnel junctions (STJs) as photon detectors has received attention in recent years as STJs offer high spectral resolution, single photon counting, and good quantum efficiency for low-light applications at a variety of wavelengths.¹ These detectors operate by counting the number of quasiparticle excitations that are produced when a photon is absorbed. In order to operate, the STJ detector must be biased at a voltage V less than the gap voltage $V_{\text{gap}}=2\Delta/e$, where 2Δ is the energy gap of the superconductor and e is the electron charge. Voltages in this range are usually referred to as subgap voltages. Biasing of a detector junction in the subgap is usually achieved by applying a magnetic field parallel to the tunnel barrier. While not difficult in practice, the elimination of the magnetic field could open up new applications for the STJ detector and ease constraints in fabricating large arrays.²

In a recent paper, we proposed a new biasing scheme for the STJ detector that could potentially eliminate the need for a magnetic field.³ In this scheme, a single detector junction is replaced by a circuit of three junctions, with one of the three junctions functioning as the detector. In the correct biasing state, which is achieved by first increasing and then decreasing the applied current, the detector junction is held at a subgap voltage through interaction with the other two junctions; no applied magnetic field is necessary. In this paper, we present experimental current-voltage (I - V) measurements that demonstrate this idea.

The paper is organized as follows. In Sec. II, we present the details of the experiments and the devices tested. In Sec.

III, we show measurements of the subgap current for a *single* junction by applying a parallel magnetic field. By fitting these data, we obtain a *quantitative* relationship for the I - V characteristics in the subgap range for our junctions. This relationship is then used to model the three-junction measurements. In Sec. IV, we present measurements of a three-junction circuit and model the movement of the detector junction's operating point as we vary the junction to which the current is applied and the operating temperature. Comparisons between theory and experiment are shown. These measurements demonstrate that we have obtained the correct biasing state. Finally, in Sec. V, we present conclusions and outlook for use in future detectors.

II. EXPERIMENTS AND SAMPLES

The measurements were conducted on junctions fabricated at a current density of 30 A/cm² by Hypres, Inc.⁴ One single junction device (labeled 1J-1) and two different three-junction devices (labeled 3J-1 and 3J-2) were studied in detail. The three-junction devices have the three junctions in a superconducting rectangular loop of $110 \times 150 \mu\text{m}^2$; the size of the loop was found to be unimportant in our previous theoretical study.³ Table I lists the parameters of the different junctions. The single junction device was diamond shaped to reduce the amount of parallel magnetic field necessary to suppress the Josephson supercurrent. For the three-junction devices, the different junctions are labeled A, B, and C. Junction A is the largest junction and has a relative size of 1.0, while junctions B and C have relative sizes of either 0.5 or 0.3. The critical current, I_{crit} , scales proportionally with area. In our original designs, Junction C was designated as the detector junction; thus, to facilitate comparison, it is also diamond shaped. The single junction device 1J-1 was on the same physical chip as the three-junction device 3J-1 and was

^{b)}Electronic mail: ksegall@mail.colgate.edu.

^{a)}Present address: Department of Applied Physics, Yale University, New Haven, CT 06520-8284.

TABLE I. Device and junction parameters.

| Device | Type | Junction | Shape | Dimensions | Area | I_{crit} | Rel. size |
|--------|----------------|----------|---------|----------------------------------|----------------------|-------------------|-----------|
| 1J-1 | Single | A | Diamond | $20 \times 10 \mu\text{m}^2$ | $100 \mu\text{m}^2$ | $30 \mu\text{A}$ | 1.0 |
| 3J-1 | three-junction | A | Square | $57.8 \times 57.8 \mu\text{m}^2$ | $3341 \mu\text{m}^2$ | $995 \mu\text{A}$ | 1.0 |
| | | B | Square | $40.8 \times 40.8 \mu\text{m}^2$ | $1665 \mu\text{m}^2$ | $500 \mu\text{A}$ | 0.5 |
| | | C | Diamond | $63.1 \times 31.5 \mu\text{m}^2$ | $994 \mu\text{m}^2$ | $298 \mu\text{A}$ | 0.3 |
| 3J-2 | three-junction | A | Square | $44.7 \times 44.7 \mu\text{m}^2$ | $1998 \mu\text{m}^2$ | $600 \mu\text{A}$ | 1.0 |
| | | B | Square | $31.7 \times 31.7 \mu\text{m}^2$ | $994 \mu\text{m}^2$ | $298 \mu\text{A}$ | 0.5 |
| | | C | Diamond | $63.1 \times 31.5 \mu\text{m}^2$ | $994 \mu\text{m}^2$ | $298 \mu\text{A}$ | 0.5 |

measured in the same cooldown. The three-junction device 3J-2 was on a different chip and was measured in a different cooldown. The sizes and areas listed have an uncertainty of a few percent due to the process bias of the Hypres fabrication.

The measurements conducted were straightforward measurements of the I - V curves at different temperatures. All experiments were performed from a temperature of $T = 0.25$ K to about $T = 2.5$ K in a pumped ^3He refrigerator. The single junction device was current biased with a voltage source and a $500 \text{ k}\Omega$ resistor. A magnetic field of about 13 G was applied parallel to the junction in order to suppress the Josephson supercurrent. Figure 1 shows the electrical biasing schemes used in the three-junction device measurements. The three-junction devices were biased with a $2 \text{ k}\Omega$ resistor and no applied magnetic field. A total current I_T was applied to the circuit; its value was determined by measuring the voltage across the bias resistor. Junction voltages were measured directly across two of the junctions (V_A and V_C), while the remaining voltage (V_B) was determined from Kirchhoff's voltage law, $V_B = V_A + V_C$. Note that I_T represents the total current flowing in the circuit; the current division between junction B and junctions A and C is not measured directly, but rather inferred from the modeling (see Sec. IV). Voltages were measured with a Burr-Brown INA110 instrumentation amplifier, digitized with a National Instruments PCI card, and saved on disk.

In the three-junction devices, all of the junctions were fabricated with leads attached to them. It was thus possible to change the junction to which the current was applied. Our model predicts that the operating voltages in the correct biasing state should depend on their relative size. By changing the junction to which we applied the current, we were able to test these aspects of our model. Figure 2 shows the four different measurement configurations that we used. In Fig. 1,

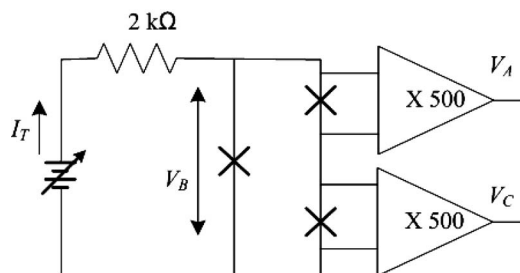


FIG. 1. Electrical biasing scheme for the three-junction devices. A current I_T was applied through a $2 \text{ k}\Omega$ bias resistor. Voltages V_A and V_C were measured directly, while V_B was computed as $V_B = V_A + V_C$.

the current was shown being applied to junction B, with the voltage measured across junctions A and C; this corresponds to configuration I in Fig. 2. The discussion below will focus first on this configuration, because the effect of the size difference between junctions A and C was the most dramatic. Later, results will be shown for all four configurations.

III. SINGLE JUNCTION MEASUREMENTS

In order to facilitate comparison with theory for the three-junction devices, the subgap current for the single junction 1J-A was first measured and analyzed. Figure 3 shows the current voltage characteristics for three different temperatures: 0.80, 2.18, and 2.50 K. The value of the subgap current in the 0.3–0.6 mV range at 2.18 K is 10 nA, about 3×10^{-4} times I_{crit} . The first Fiske step is apparent at approximately $V = 0.6$ mV, which agrees with that predicted by the size of the junction.⁵ Also shown in figure are the fits to theory. The theoretical current is determined from two processes: superconductor-insulator-superconductor (SIS) tunneling between two superconductors of the same energy gap and a small amount of superconductor-insulator-normal (SIN) tunneling, likely due to normal regions of trapped flux near the tunnel barrier. The total current is obtained from a weighted sum of these two currents, I_{SS} and I_{SN} , and a third current, I_{gap} , to account for the current rise at V_{gap} due to broken Cooper pairs.

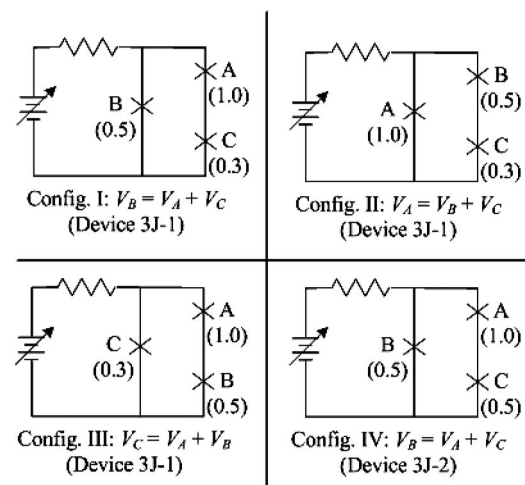


FIG. 2. Different measurement configurations. The current is applied at different places in the circuit, giving a chance to test the model in different ways. The relative junction sizes are given in parentheses. The discussion in the text focuses mostly on configuration I.

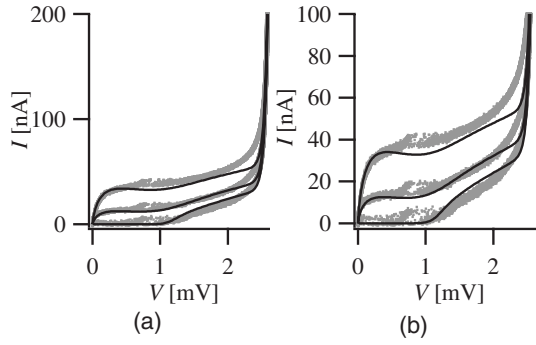


FIG. 3. Current vs voltage on two different scales for the single junction 1J-1 at $T=0.80$ K (lowest curve), 2.18 K (middle curve), and 2.50 K (highest curve). The gray points are data and the solid black lines are fits to Eqs. (1)–(4), using the parameters in Table I.

I_{SS} is given by the BCS quasiparticle current for tunneling between two superconductors of equal energy gaps,⁶

$$I_{SS} = \left(\frac{2}{eR_N} \right) (eV + \Delta) \times \left(\frac{2\Delta}{eV + 2\Delta} \right)^{1/2} \exp\left(\frac{-\Delta}{kT} \right) \sinh\left(\frac{eV}{2kT} \right) K_0\left(\frac{eV}{2kT} \right). \quad (1)$$

Here R_N is the normal-state resistance of the junction, k is Boltzmann's constant, and K_0 indicates the zeroth-order modified Bessel function. The value of R_N is calculated from the critical current using the Ambegaokar and Bartoff relationship.⁷

I_{SN} is given by an integral over energy,⁶

$$I_{SN} = \frac{1}{eR_N} \int_{-\infty}^{\infty} \frac{E'}{(E'^2 - V_0^2)^{1/2}} [f(E' - eV) - f(E')] dE'. \quad (2)$$

Here E' is a variable of integration, $f(E')$ and $f(E' - eV)$ are the Fermi functions evaluated at E' and $E' - eV$, respectively, and the range of integration excludes $|E'| < \Delta$. The parameter V_0 represents the gap of the superconducting material from which the quasiparticles are tunneling. We found V_0 to be slightly less than Δ_{Nb} , probably due to the thin aluminum deposition in the niobium trilayer fabrication process. I_{SN} is multiplied by a factor β in the expression for the total current, where β represents the strength of the SIN tunneling relative to the SIS tunneling ($\beta \ll 1$).

The current I_{gap} is given by the following empirical expression:

$$I_{\text{gap}} = \left\{ 1 - \tanh \left[\alpha \left(1 - \frac{eV}{2\Delta} \right) \right] \right\} \frac{V}{2R_N}. \quad (3)$$

This term is equal to zero if $eV \ll 2\Delta$ and equal to (V/R_N) if $eV \gg 2\Delta$; this functional form has been used elsewhere.⁸ The value of α gives the width of the current rise at $(2\Delta/e)$, with larger values of α giving a sharper rise in current. It is chosen to match experiment.

The total current I is then given by

$$I = I_{SS} + \beta I_{SN} + I_{\text{gap}}. \quad (4)$$

The fits to Eqs. (1)–(4) are shown in Fig. 3, showing good agreement. The fitting parameters for the model are Δ , α , β ,

TABLE II. Fitting parameters.

| Device | Δ | V_0 | β | α | Figure |
|--------|----------|---------|----------------------|----------|-----------------|
| 1J-1 | 1.425 mV | 1.15 mV | 8.0×10^{-4} | 30 | Fig. 3 |
| 3J-1 | 1.34 mV | 1.22 mV | 7.0×10^{-4} | 40 | Figs. 7(a)–7(c) |
| 3J-2 | 1.34 mV | 1.30 mV | 5.5×10^{-4} | 35 | Fig. 7(d) |

and V_0 . The parameter values used in Fig. 3 are given in Table II.

The value of $\beta \sim 10^{-3}$ indicates that the SIN tunneling is very small as compared to the SIS tunneling. No attempt was made to change the amount of SIN tunneling by heating and cooling in different fields or by improving the magnetic shielding; this remains an issue for future work. However, knowing the amount of SIN tunneling gives us a functional form for a single I - V curve and allows us to proceed with our study of the subgap biasing state.

IV. JUNCTION MEASUREMENTS

Because no magnetic field is applied in the three-junction measurements, the current-voltage characteristics for the three-junction devices are hysteretic. Thus, the I - V curves are different depending on whether the current is increasing from zero or decreasing from large current values (greater than several times V_{gap}/R_N). In our previous numerical studies, we found that increasing the current led to somewhat complex switching dynamics, whereas decreasing the current resulted in simpler dynamics that could be described by a basic dc model. Our experiments confirmed this. In this section we show the results for the three-junction devices, focusing first on increasing the current and then on decreasing the current.

Figure 4(a) displays the I - V characteristics measured in configuration I. Plotted is the total current I_T versus the three different junction voltages. Upon increasing the current, junctions B and C switch first at an applied current of about 0.5 mA. For currents larger than this but smaller than about 2.3 mA, junctions B and C stay in the voltage state while junction A is in the superconducting state. At about $I_T = 2.3$ mA, junction A switches into the voltage state. At this

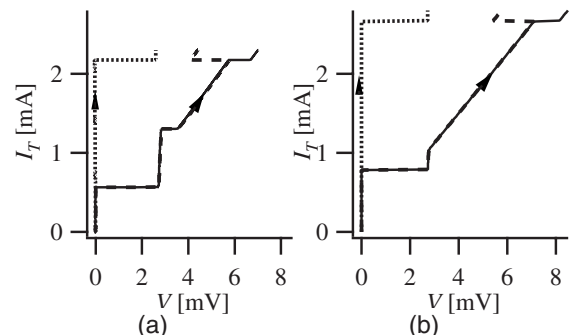


FIG. 4. I - V curve for experiment (a) and theory (b) while increasing the applied current in configuration I. V_A is the dotted line, V_B is the solid line, and V_C is the dashed line. Junctions B and C switch first, while junction A switches last.

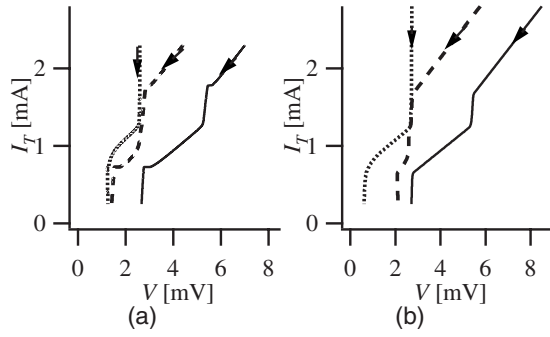


FIG. 5. I - V curve for experiment (a) and theory (b) while decreasing the applied current in configuration I. V_A is the dotted line, V_B is the solid line, and V_C is the dashed line. In the experiment, the applied current is decreased until at about 0.25 mA; at this point the detector state has been reached and the current is held constant.

point V_C decreases while V_B increases in order to maintain $V_B = V_A + V_C$. For applied currents greater than 2.3 mA, all three junctions are in the voltage state.

In order to predict the form of the I - V curve for increasing the current, a full time-dependent model must be applied. The complete Resistive and Capacitive Shunted Junction (RCSJ) form of the current is used for each junction and the system equations are obtained by current conservation and fluxoid quantization. Such a model was explained previously.³ The results of this model are shown in Fig. 4(b). As can be seen, the qualitative features of the dynamics—the order of the junction switching and the general shape of the I - V curves—are reproduced by the model.

After all the junctions have switched to the voltage state, the system is in a full whirling mode. If the current is now decreased, the system follows a different path than it did when the current was increased, as shown in Fig. 5(a). Kirchhoff's voltage law continues to require that $V_B = V_A + V_C$. Figure 5(b) shows the predictions of the full model, again showing good qualitative agreement.

In the experiments, the applied current was decreased to a certain value and then held constant. At this point the system has reached the detector biasing state; junctions A and C are biased in the subgap. This bias point is experimentally stable over time and does not retrap, as it does when decreasing the bias current in a single junction. The time stability was not measured directly, but the state was stable on the order of an hour as we performed our measurements. The state also seemed stable against small amounts of bias voltage and temperature fluctuations; no study was done to see how stable it was against parasitic interference. Our numerical study showed that the biasing state is theoretically stable for potentially very long periods of time.³

The fact that junctions A and C are now biased in the subgap is perhaps not fully convincing from Fig. 5. Although V_A and V_C are less than V_{gap} , the total current flowing in the circuit is still of order I_{crit} , whereas the subgap current is of order $10^{-4} I_{\text{crit}}$, as measured in Sec. III. What is actually occurring is that nearly *all* of the bias current I_T is flowing through junction B, while only the small subgap current is flowing through junctions A and C. We now attempt to show this by tracking the changes in the operating point as we vary

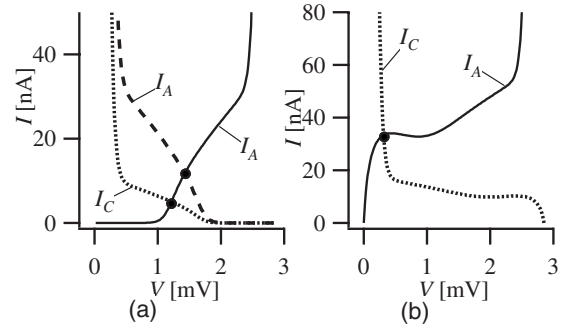


FIG. 6. (a) dc model for configuration I at $T=0.8$ K. For junction A, I_A vs V_A is plotted as a solid line. The reflected I - V curve for junction C, I_C vs $(V_{\text{gap}} - V_A)$ is plotted as a dotted line; here we make use of the fact that $V_C = V_{\text{gap}} - V_A$. Since the currents I_A and I_C are equal, the curves intersect at the operating voltage V_A . For comparison, the reflected I - V curve for junction A is shown as a dashed line; this corresponds to the case where junctions A and C are the same size. In this case, the operating point would be at $V_A = V_{\text{gap}}/2$. Because junctions A and C are not the same size, the operating voltage V_A instead lies at a value less than $V_{\text{gap}}/2$. (b) dc model for configuration I at 2.5 K. The larger temperature enhances the effect of the size difference. The curves now intersect at an even smaller value of V_A .

the junction to which current is applied and the operating temperature.

When decreasing the current, the full time-dependent model is no longer necessary. A simpler dc model, using only Kirchhoff's voltage and current laws, describes the circuit dynamics well. This model is given for configuration I as

$$V_B = V_A + V_C, \quad (5)$$

$$I_A(V_A) = I_C(V_C), \quad (6)$$

$$I_T = I_A(V_A) + I_B(V_B). \quad (7)$$

The functions $I_A(V_A)$, $I_B(V_B)$, and $I_C(V_C)$ are equal to the function $I(V)$ given by Eqs. (1)–(4). The functions differ only in that the different-sized junctions have different values of the normal-state resistance R_N . Equations (5)–(7) are for the circuit of configuration I; for configurations II–IV, junctions A, B, and C change places appropriately. After decreasing the current, the voltage V_B is approximately equal to a constant value V_{gap} , so we can approximate Eq. (5) with $V_{\text{gap}} = V_A + V_C$. Rearranging this we find that $V_C = V_{\text{gap}} - V_A$. Now, Eqs. (5)–(7) can be solved graphically by plotting the I - V curve for junction A, $I_A(V_A)$, and the reflected I - V curve for junction C, $I_C(V_{\text{gap}} - V_A)$, on the same axis. Since the currents I_A and I_C are equal, the curves intersect at the operating voltage V_A . This is done in Fig. 6(a) for $T=0.8$ K. The intersection of the two points gives the solution $V_A \approx 1.25$ mV. Since V_{gap} is about 2.8 mV, this gives $V_C \approx 1.55$ mV. We now consider how this operating point (V_A , V_B , V_C) varies as we change where the current is applied and the operating temperature.

First, we consider the effect of differing junction sizes. Also plotted in Fig. 6(a) is the reflected curve for I_A , $I_A(V_{\text{gap}} - V_A)$, as a dashed line. This would represent the case when junctions A and C are the same size. In that case, the two curves would intersect at an equal voltage where $V_A = V_C = V_{\text{gap}}/2$. This point is indicated in Fig. 6(a). However, since junction C is smaller than junction A, I_C is less than I_A

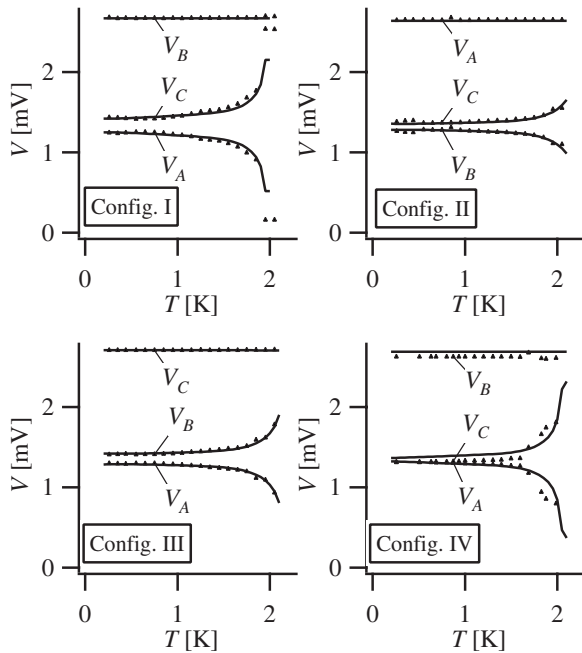


FIG. 7. Operating voltages vs temperature for configurations I, II, III, and IV. The points are measurements and the solid line is the theory from the dc model. Of the two junctions biased in the subgap, the smaller junction always lies at a higher voltage. At low temperatures, the operating point is independent of temperature. At higher temperatures, the effect of the size differences is enhanced, resulting in the spreading seen in the plots.

at a given voltage. The intersection of the two curves occurs more to the left, at a smaller value of V_A . Thus, the operating point is at a smaller voltage for junction A and a larger voltage for junction C than if the two junctions were the same size.

Next we consider the effect of changing temperature. Figure 6(b) shows the same model again for configuration I, but now for $T=2.5$ K. Because of the size difference between junctions A and C, the operating point again occurs at a lower voltage, less than $V_{\text{gap}}/2$, as in Fig. 6(a). The larger temperature simply enhances the effect, moving the operating point even further to the left than it was at 0.8 K. Junction C now sits on the gap rise, while junction A sits in the low voltage thermal part of the I - V curve. As the temperature is increased, the operating point continues moving toward larger values of V_C and smaller values of V_A .

In Fig. 7 we now present the full measurements of the operating point versus temperatures for the four different configurations described in Fig. 2. In each case, the graphs show similar trends. At low temperatures, the operating point is independent of temperature. Of the two junctions biased in the subgap, the larger-sized junction always sits at a lower voltage, while the smaller-sized junction is at a higher voltage. Thus, in configuration II we have $V_C > V_B$, in configuration III we have $V_B > V_A$, and in configurations I and IV we have $V_C > V_A$. As the temperature increases, the difference in the two subgap voltages also increases, resulting in the “spreading” seen in all four plots.

Also shown in Fig. 7 are the fits from the dc model [Eqs. (5)–(7)]. The fitting parameters for the three different devices are shown in Table II. The parameters are all very similar. The value of Δ is close to the expected value of 1.4 mV for

Nb, and the value of V_0 is slightly less than 1.4 mV. The value of β indicates that the SIN tunneling is much weaker than the SIS tunneling.

From the excellent agreement between experiment and theory in Fig. 7, it is clear that the subgap biasing state has been reached. It is also clear that the dc model describes the movement of the operating point quite well. Device 3J-1 was measured in three different configurations (configurations I, II, and III) and the fits were obtained with a single set of fitting parameters.

V. CONCLUSIONS

We have demonstrated stable biasing of a STJ at subgap voltages without a magnetic field. By first measuring the subgap current of a single junction, we were able to establish a functional form of the current versus voltage for our junctions. Using that functional form, we were able to fit the operating point of a three-junction circuit and model its movement as we varied temperature and the junction to which current was applied.

The subgap biasing state is achieved by first increasing and decreasing this hysteric dynamics is due to the nonlinearity of the junctions in the circuit. These dynamics are similar to a nonlinear mode called a discrete breather, which can exist in a Josephson ladder.⁹ A type B breather⁹ has junction voltages of V_g , $V_g/2$, 0, and $V_g/2$ going around a loop; the subgap voltages of $V_g/2$ occur without a magnetic field. These experiments motivated our design for the biasing circuit. A three-junction circuit in a single cell displaying breatherlike states and subgap voltages was reported in a more recent work;¹⁰ we chose to pursue our design because the breatherlike states in those experiments need the application of a second bias current to be excited. To the best of our knowledge, the nonlinear subgap biasing state we have shown is not achievable by replacing any of the three junctions with a resistor.

The possible implications for STJ detectors have been discussed in our previous work, and that discussion remains relevant after these experiments.³ While the subgap state clearly exists, it will still take some work to construct a practical detector with magnetic-field-free biasing. The main issue is the dynamic resistance. Two junctions are biased in the subgap (for example, A and C in configuration I); presumably, the photon-induced current will flow out of only one of them (junction C). The read-out amplifier will then see the parallel resistance of the two junctions A and C. For experiments at higher photon energies, where the amplifier noise can typically be made smaller than intrinsic fluctuations, this will most likely not have a severe impact; at lower photon energies, it may matter more. However, now that the biasing state has been demonstrated, there are other possibilities open to consideration. For example, one could measure the voltage change due to a photon directly, instead of measuring the current, as is done in most existing experiments. One could also allow *both* junctions biased in the subgap (e.g., junctions A and C in configuration I) to be exposed to photons, and read out both signals. This would allow for a greater reduction in amplifier leads. These two junctions

could perhaps be the two junctions in a distributed-readout-type of detector.¹¹ The power dissipation by the biasing junction, for example, junction B in configuration I, is of order $P=IV\sim 1\ \mu\text{W}$. Most cryogenic systems have a cooling power of order 10–100 μW , so this is not necessarily a big problem as far as heat is dissipated in the bath. The heat from the biasing junction could locally heat up one of the other two junctions, although it appears that this did not happen in our measurements. If local heating is a problem, the biasing junction could be put on a membrane with the substrate etched away. These and other issues will need to be sorted out in future experiments.

ACKNOWLEDGMENTS

We thank T. P. Orlando and D. E. Prober for useful discussions. K.S. acknowledges the Colgate Division of Natural Sciences for funding; J.J.M. is supported by the Spanish DGICYT Contract No. FIS2005-00337.

- ¹J. Mather, *Nature (London)* **401**, 654 (1999); N. E. Booth and D. J. Goldie, *Supercond. Sci. Technol.* **9**, 493 (1996).
- ²For example, another class of detectors, Transition Edge Sensors, are used in electron microscopy; see, for example, D. A. Wollman, S. W. Nam, G. C. Hilton, K. W. Irwin, N. F. Bergren, D. A. Rudman, J. M. Martinis, and D. E. Newbury, *J. Microsc.* **199**, 37 (2000). However, STJs would presently not be feasible in such an application, since the applied magnetic field would affect the electron beam.
- ³K. Segall, J. J. Mazo, and T. P. Orlando, *Appl. Phys. Lett.* **86**, 153507 (2005); K. Segall, J. J. Mazo, and T. P. Orlando, *IEEE Trans. Appl. Supercond.* **15**, 583 (2005).
- ⁴Hypres, Inc., Elmsford, NY, www.hypres.com.
- ⁵M. D. Fiske, *Rev. Mod. Phys.* **36**, 221 (1964).
- ⁶T. Van-Duzer and C. W. Turner, *Principles of Superconductive Devices and Circuits* (Edward Arnold, London, UK, 1981).
- ⁷V. Ambegaokar and A. Baratoff, *Phys. Rev. Lett.* **10**, 486 (1963).
- ⁸E. Trias, J. J. Mazo, A. Brinkman, and T. P. Orlando, *Physica D* **156**, 98 (2001).
- ⁹E. Trias, J. J. Mazo, and T. P. Orlando, *Phys. Rev. Lett.* **84**, 741 (2000); P. Binder, D. Abraimov, A. V. Ustinov, S. Flach, and Y. Zolotaryuk, *ibid.* **84**, 745 (2000).
- ¹⁰F. Pignatelli and A. V. Ustinov, *Phys. Rev. E* **67**, 036607 (2003).
- ¹¹M. Furlan, E. Kirk, and A. Zehnder, *J. Appl. Phys.* **101**, 054501 (2007).